Modeling Cement Placement Using a New 3-D Flow Simulator

Mark Savery, Wilson Chin, and Krishna Babu Yerubandi, Halliburton

Abstract

The paper presents a new computational fluid dynamics (CFD) simulator that models multiple aspects of mud displacement during cementing. In 2001, Crook et al. published an article[1] describing the "eight steps" to ensure successful cement jobs. The top five steps relate directly to the success of cement slurry placement, and never before has a simulator been able to model all five together. The present simulator dynamically models, in three dimensions (3-D), the intermixing of wellbore fluids in both pipe and annuli with casing movement during hole cleaning and cement slurry placement.

The real value simulation brings is that the user can 'practice' with the simulator before going to the rig site. Life does not occur in two dimensions, and this 3-D simulator can help operators and engineers make better decisions to avoid cement job failure, improve well integrity, and control rig time cost associated with squeeze workovers. Its interactive 3-D visualizer allows the user to screen various scenarios and helps create the best design on the first try, to avoid costly remedial work later.

Introduction

In completion of oil and gas wells, cementing operations are employed to provide zonal isolation. Perhaps the most important factor engineers and operators should consider for successful cementing is adequate drilling fluid removal. Efficient mud displacement is perhaps the most important factor in helping ensure a successful cement job. To help optimize mud removal, the primary technique used is to pump a spacer fluid with modified rheology that creates a favorable fluid-fluid interface to enhance mud displacement. In many instances, it is highly desirable to monitor how this interface evolves over time. Fluid intermingling may inhibit the capability of a fluid to perform its intended purpose, for example, intermixing of spacer fluid with cement slurry may lead to contamination of the cement. This contamination may cause an undesirable failure of the setting of the cement and, consequently, a significant increase in cost due to increased wait time or remedial repair.

Several other factors that directly impact mud displacement are wellbore geometry, mud conditioning, casing movement via reciprocation and rotation, casing centralization, and optimizing the pump rate.[2] However, often unknown is the extent to which these variables affect mud displacement, especially when applied in combination with one another. Even a relatively straightforward cementing operation can quickly become a challenging scenario with multiple variables. The industry has conducted numerous large-scale physical studies[3-8] over the last half-century to empirically evaluate the importance of these factors on displacement efficiency.

More recently, however, several studies have taken advantage of computational numerical methods to describe the different aspects of the mud displacement process in annular geometries. Tehrani et al.[9] discussed combined theoretical and experimental studies of laminar displacement in inclined eccentric annuli by appropriately coupling the momentum equation with the concentration equation suggested earlier by Landau and Lifshitz.[10] Cui and Liu[11] addressed helical flow in eccentric annuli based on the bipolar coordinate system. Pelipenko and Frigaard[12] examined fluid-fluid displacement in a two-dimensional "narrow annuli" without casing reciprocation or rotation. The well known model discussed by Escudier et al[13,14] considered non-Newtonian viscous helical flow in eccentric annuli for a single fluid. Dutra et al.[15] analyzed the interface between adjacent fluids through three-dimensional annular eccentric tubes using a commercial computational fluid dynamics (CFD) package. Finally, Li and Novotny[16] proposed a Lattice-Boltzmann approach based on single fluid flow between two parallel plates to describe cement displacement behavior.

While a significant amount of noteworthy work has been done in the past, the current authors' attempt to build a comprehensive CFD model that accounts for all physical parameters known to affect displacement phenomena, namely pump-rate adjustments, fluid-fluid intermixing and diffusion, casing standoff, abnormal wellbore geometries, fluid rheology, wellbore deviation, casing reciprocation, and casing rotation. Therefore, a three-dimensional simulator capable of modeling these scenarios has been developed. The computational system is formulated on a general curvilinear coordinate system whose boundaries can conform to irregular boreholes such as those with washouts. Unlike existing models limited to weakly eccentric annuli without casing movement, the present simulator handles multiple real-world effects and efficiently performs trade-off studies that can enable more economical and effective cementing jobs while helping ensure the longevity of the well.

Theory

We consider the transient and eventual steady-state flow of the miscible mixing of Newtonian or non-Newtonian fluids in general eccentric annular borehole geometry with localized washouts possible along the axial direction. The numerical solution to our formulation predicts important operational properties such as mixing zone thickness, location and time scales, evolving velocity, viscosity and density spatial distributions, and so on, as functions of geometry, fluid rheology, initial conditions, and casing reciprocation and rotation. The mathematical approach is best described conceptually starting from simpler illustrative flow limits.

Baseline Equations

The general non-Newtonian rheological equations for unsteady single-phase fluid flow of constant density ρ with and without yield stress are given by

$$\rho\,(\partial v_r/\partial t + v_r\,\partial v_r/\partial r + v_\theta\,/r\,\partial v_r/\partial\theta\ - v_\theta^2/r + v_z\,\partial v_r/\partial z) =$$
$$= F_r - \partial p/\partial r + 1/r\,\partial(r S_{rr})/\partial r + 1/r\,\partial S_{r\theta}/\partial\theta - 1/r\,S_{\theta\theta} + \partial S_{rz}/\partial z \quad (1)$$

$$\rho\,(\partial v_\theta/\partial t + v_r\,\partial v_\theta/\partial r + v_\theta\,/r\,\partial v_\theta/\partial\theta\ + v_r v_\theta/r + v_z\,\partial v_\theta/\partial z) =$$
$$= F_\theta - 1/r\,\partial p/\partial\theta + 1/r^2\,\partial(r^2 S_{\theta r})/\partial r + 1/r\,\partial S_{\theta\theta}/\partial\theta + \partial S_{\theta z}/\partial z \quad (2)$$

$$\rho\,(\partial v_z/\partial t + v_r\,\partial v_z/\partial r + v_\theta\,/r\,\partial v_z/\partial\theta\ + v_z\,\partial v_z/\partial z) =$$
$$= F_z - \partial p/\partial z + 1/r\,\partial(r S_{zr})/\partial r + 1/r\,\partial S_{z\theta}/\partial\theta + \partial S_{zz}/\partial z \quad (3)$$

$$\partial v_r/\partial r + v_r/r + 1/r\,\partial v_\theta/\partial\theta + \partial v_z/\partial z = 0 \quad (4)$$

where v_r, v_θ and v_z are radial, azimuthal, and axial velocity components in a cylindrical radial coordinate system, p is pressure, F_r, F_θ and F_z are body forces, noting that $\underline{S} = 2\,N(\Gamma)\,\underline{D}$ denotes the deviatoric stress tensor, with $N(\Gamma)$ being the apparent viscosity function and Γ the shear rate. Here, $\underline{D}$ is the deformation tensor in cylindrical radial coordinates.

Equations 1-4 are four nonlinearly coupled transient partial differential equations in the four unknowns v_r, v_θ, v_z and p. The first three represent momentum equations and the fourth the continuity equation. To obtain practical solutions, simplifications must be made that are consistent with actual borehole flow applications. In most problems, the radial velocity is much smaller than both axial and azimuthal velocities, and so, the radial momentum equation can be ignored. We also ignore the azimuthal pressure gradient in the tangential momentum equation because this induced effect is small relative to the dragging motion associated with casing rotation. This leaves Equations 2 and 3 as coupled governing equations driven by a (time and space varying) axial pressure gradient $\partial p/\partial z$. Auxiliary conditions are required to complete the formulation. For example, as initial conditions, one might have quiescent flow when starting from rest, but here, we consider uniform velocities in the case of quasi-steady flows due to positive displacement pumps. No-slip velocity boundary conditions apply at all solid surfaces, e.g., zero velocities at borehole walls and prescribed rotation and axial reciprocation motions at the casing surface. In general, the

equations are integrated by a finite difference time-marching scheme.

Curvilinear Coordinates

The foregoing equations are written in cylindrical radial coordinates; however, this does not imply that only concentric problems can be solved. Any geometry can, in principle, be modeled. The initial baseline polar formulation is chosen because it allows rotation rate boundary conditions to be conveniently expressed at the circular casing surface. But concurrently, we do not require the borehole contour to take the form of a concentric circle; it may be eccentric and contain large washout or fracture modifications or any geometric perturbations as determined from caliper logs. To accommodate this geometric flexibility, the above governing equations are next transformed from (r,θ,z) coordinates to Cartesian (x,y,z) variables using standard polar coordinate transforms. They are then further re-expressed in general boundary-conforming curvilinear coordinates (ξ,η,z) using the $x(\xi,\eta,z)$ and $y(\xi,\eta,z)$ numerical mapping procedure developed in Chin.[17] The latter method transforms any doubly connected region into a simple rectangular domain for computational convenience to provide improved physical resolution in tight spaces as needed. For illustrative purposes, Fig. 1 shows a borehole with a Texas-shaped boundary and an internal fracture slit which is mapped into the actual grid. Using this method, it is possible to represent any borehole shape containing, for example, washouts or localized fractures.

Miscible Flow Extension

The transformed equations thus far apply to single-phase fluids only. To extend the formulation to two-phase flow for miscible mixing applications, we now require an additional dependent variable, namely, the fluid concentration function $C(\xi,\eta,z,t)$. This physical quantity satisfies a transformed convective-diffusive partial differential equation of the form

$$\partial C/\partial t + \mathbf{q}_{(\xi,\eta,z)} \bullet \nabla C = \varepsilon\,\{C_{zz} + (\alpha C_{\xi\xi} - 2\beta C_{\xi\eta} + \gamma C_{\eta\eta})\,/J^2\} \quad (5)$$

where the transport velocity $\mathbf{q}_{(\xi,\eta,z)}$ contains both axial and azimuthal components needed to establish helical flow and ε is a diffusion coefficient. Note that this diffusion equation does not explicitly contain transport parameters like viscosity, but that such effects appear indirectly through the vector velocity $\mathbf{q}$ satisfying Equations 1-4. Various coefficients in the foregoing fluid description must also be extended to handle its additional degrees of freedom. For example, the previously constant fluid density ρ may now take the variable form $\rho = C\rho_1 + (1-C)\,\rho_2$ so that $\rho = \rho_1$ when $C = 1$ and $\rho = \rho_2$ when $C = 0$ where "1" and "2" might individually represent mud, spacer fluid, or cement slurry. The stress tensor $\underline{S} = 2\,N(\Gamma)\,\underline{D}$ used in single-phase fluid must be similarly modified. For example, the constant viscosity μ in the Newtonian limit is replaced by an empirically determined function $\mu(C)$ guided by laboratory experiments – this function would, of course, satisfy the limits $\mu = \mu_1$ when $C = 1$ and $\mu = \mu_2$ when $C = 0$. For Herschel-

Bulkley fluids, similar comments would apply to the constants n, K and τ_{yield}. Example mixing functions determined in the laboratory for typical fluid combinations and used in the present simulations are shown in Fig. 2 as surface plots that depend on concentration and shear rate. This miscible flow extension of the conventional single-phase formulation was first given conceptually by Landau and Lifshitz.[10] It is implemented here for three-dimensional annular flows within the curvilinear coordinate framework. Because the structure of the transformed stress terms is extremely complicated, the transient integration method used is explicit in time. In the quasi-steady examples presented here, the total volume flow rate is specified for the problem; in this limit, the pressure gradient used in the axial momentum equation is approximately the one obtained on a steady two-dimensional basis.

Simulator Capabilities

To assess the capabilities of the simulator, a series of demonstrations is presented here:

1. Eccentric annular flow
2. Mixing zone thickness and channel length
3. Casing rotation

The same baseline inputs are used in each simulation:

Borehole Diameter	= 6.5 in. (16.5 cm)
Casing Diameter	= 4.5 in. (11.4 cm)
Length/Depth	= 400 ft (122 m)
Pump Rate	= 2 bbl/min (0.32 m^3/min)
App. Visc. Displaced Fluid	= 20-cP
App. Visc. Displacing Fluid	= 30-cP
Density Displaced Fluid	= 10-lb/gal (SG = 1.2)
Density Displacing Fluid	= 11.7-lb/gal (SG = 1.4)

Fig. 3 shows the baseline 2-D radii grid and Fig. 4 shows the baseline 3-D wellbore grid. Other input parameters such as standoff percentage, the diffusion coefficient, and casing movement speeds were modified depending on the study performed. Simulations were conducted in vertical annuli only. For all demonstrations, the fluid being displaced (e.g. mud) is characterized by the color blue and the displacing fluid (e.g., spacer or cement) is characterized by the color red. The legend representing the degree of mixing between the two fluids is designated by Fig. 5. Note that on many of the subsequent figures, a dark orange color is used to describe a displacing fluid concentration of 97%. This is an arbitrary value for visual description only; any other concentration value may be selected according to the user's preference.

Eccentric Annular Flow

Fluid flow in a wellbore annuli is rarely, if ever, an exactly concentric situation (i.e., a perfectly circular casing string set exactly centered in a perfectly circular borehole). In reality, the casing or liner is often offset closer to one side of the

borehole, leaving an eccentric annulus with a distinct wide side and narrow side. In addition, the borehole itself may be oval-shaped or have extreme variances in geometry due to washout sections. It is often difficult to predict the top-of-cement (TOC) with these variations, so one of the benefits of the simulator is its capability to estimate TOC whatever geometry may be. This estimation becomes increasingly important when the casing or liner is offset and fluid flow is slower up the narrow annular side, leaving a long, uncemented section. If this occurs, remedial squeeze cementing may be required.

The theory behind the simulator code is designed to account for abnormal geometric variations, and two such cases will be presented here. First, a series involving one fluid displacing another fluid in varying degrees of eccentric annuli is described. To describe the effect of offset casing, three simulations were run: The first at a typical standoff of 70% (Fig. 6), the second at a poor standoff of 40% (Fig. 7), and the third at a drastic standoff of 10% (Fig. 8), which may occur in a highly deviated well. As expected, Figs. 6-8 show the varying response of annular flow as a function of offset casing. Both the 70% case and 40% case clearly show flow on both the wide side and narrow side of the annulus (albeit to a lesser degree for the 40% case), but the extreme case of 10% shows little-to-no flow on the narrow side. In addition, Fig. 9 shows the discrepancy in velocity profiles between the narrow side (represented by the red line) and wide side (represented by the blue line) in the 70% standoff case. These demonstrations stress the need of casing centralization. Without it, flow on the wide side will dominate, leaving uncemented regions on the narrow side. With an eccentric annulus, there is never a guarantee that cement returns at surface means complete coverage around the casing. The ability to predict cement slurry location in 3-D space is invaluable, especially in situations when the casing is expected to be decentralized.

Mixing Zone Thickness and Channel Length

During any given cement job, various fluids are pumped down the casing string and subsequently up the annular gap. Each liquid has its own function; for instance, a spacer fluid is used to separate the cement slurry and existing mud. It also acts as an inner-casing cleaner and annular cleaner. Rubber or foam wiper plugs are also often deployed to wipe the inner casing. Ideally, the cement slurry remains completely uncontaminated until placed at the desired location. However, in real applications, the spacer fluid gets "used up," or mixed in with the cement, mud, or usually both. Sometimes the spacer is used up before it ever turns the corner! In addition, a wiper plug often wears down before ever reaching the bottom, causing the fluids to mingle. Fluid-fluid intermixing often becomes a problem because it can leave cement strings in the casing or mud channels in the annulus, both of which are highly undesired. Thus, if the spacer fluid or wiper plug does a poor job of displacement, remedial work and extended rig time may be necessary, which increases both labor and material costs.

Understanding how the mixing interface evolves over time is of critical importance. The numerical algorithm presented here can predict the extent of contamination and intermixing over time, which 1) can help pinpoint potential causes of stringing or channeling and 2) can provide insight into reducing material cost (e.g., optimizing spacer and excess cement amounts). Over the course of displacement, the distribution of concentration at mixing interfaces may change one of two ways. The first is mechanical mixing (convection) and the second is molecular transfer (diffusion). Recall Equation 5, the coupled convective-diffusive differential equation. In real-world cement jobs, there are typically two types of wellbore fluids encountered: Water-based and oil-based. In general, oil-based fluids are immiscible with water-based fluids, thus the convective term is likely to dominate. Conversely, water-based fluids are miscible with other water-based fluids. In this case, the diffusion term likely will have a greater impact.

Therefore, to understand the full range of fluids encountered, simulations varying the diffusion coefficient were conducted in a concentric annulus. The diffusion coefficients suggested here are arbitrary for illustrative purposes. Precise diffusion coefficients may be found experimentally, perhaps in a simple, straight tube where the displacement and thickness of the frontal interface are measured in space and time. Figs. 10-12 show that varying the diffusion coefficient has a dramatic impact on the intermixing profile. Fig. 10 shows the one extreme—perhaps when a water-based spacer fluid displaces a water-based mud—where the diffusion coefficient is high (3×10^{-2} in.^{2}/sec) and diffusion forces dominate as observed by stable, flat, mixing interface. Conversely, Fig. 12 describes the other extreme–perhaps when a water-based spacer fluid displaces an oil-based mud–where the diffusion coefficient is four orders-of-magnitude lower (3×10^{-6} in.^{2}/sec) and intermixing is driven by mechanical-convective forces.

Casing Rotation

Rotating the inner casing during cement placement results in more successful primary cement jobs and reduces the probability of remedial work such as zonal isolation squeezes and liner top squeezes.[18] The present study provides a proof-of-concept visualization of rotational effects. Fig. 13 shows a steady-state velocity profile from a 2-D slice of a 70% standoff situation with casing rotation of 20 RPM. The maximum velocity point shifts to form an asymmetric profile around the eccentric annulus. This should be expected because the fastest fluid takes the path of least resistance on the wide side but now also has an azimuthal component added to its velocity due to the rotating casing. Fig. 14 shows the same simulation but in 3-D. There is no longer just axial velocity, but rather azimuthal velocity is added via the mechanical movement of the casing. A streamline following the center (i.e., tip) of the parabolic velocity profile has been added to illustrate this induced helical flow. From this, a useful observation emerges to confirm the merits of rotating the casing: Rotation helps offset the drastic variations in wide side versus narrow side flow in eccentric annuli. This has been observed in field operations for years and now can be confirmed with CFD. With this tool, the helical flow pitch and intermixing phenomena during rotation may be predicted. This can help the cement job designer evaluate the impact of rotating the casing during displacement and make a more accurate assessment of where the top-of-cement will be.

Conclusions

The proprietary three-dimensional simulator and interactive 3-D visualizer (Fig. 14) provide foundational tools to model multiple aspects of mud displacement, including key factors such as eccentric annuli, fluid-fluid mixing, and casing movement. These tools, we hope, can enable more economical and more successful cementing jobs, as well as promote efficiencies in pre-job design and post-job analysis.

Acknowledgements

Nomenclature

(ξ, η, z) = curvilinear coordinate system
α = mapping function
β = mapping function
ε = diffusion coefficient
γ = mapping function
μ = viscosity
ρ = density
τ_{yield} **=** Hershel-Bulkley coefficient
C = concentration
$\underline{D}$ = deformation stress tensor
F_r = radial body force
F_θ = azimuthal body force
F_z = axial body force
J = mapping function
K = Hershel-Bulkley coefficient
n = Hershel-Bulkley coefficient
$N(\Gamma)$ = apparent viscosity function
p = pressure
q = transport velocity
RPM = revolutions per minute
$\underline{S}$ = deviatoric stress tensor
t = time
v_r = radial velocity
v_θ = azimuthal velocity
v_z = axial velocity

References

1. Crook, R.J. et al. "Eight Steps Ensure Successful Cement Jobs," *Oil & Gas Journal* (July 2001).
2. Sauer, C.W. "Mud Displacement during the Cementing Operation: A State of the Art," SPE 14197, SPE Annual

Technical Conference and Exhibition, Las Vegas, Sept. 22-25, 1985.

3. Smith, T.R. and Ravi K.M. "Investigation of Drilling Fluid Properties to Maximize Cement Displacement Efficiency," SPE 22775, SPE Annual Technical Conference, Dallas, Oct. 6-9, 1991.

4. Keller, S.R. et al. "Problems Associated with Deviated-Wellbore Cementing," SPE 11979, SPE Annual Technical Conference and Exhibition, San Francisco, Oct. 5-8, 1983.

5. Haut, R.C. and Crook, R.J. "Laboratory Investigation of Lightweight, Low-Viscosity Cementing Spacer Fluids," SPE 10305, SPE Annual Technical Conference and Exhibition, San Antonio, Oct. 5-7, 1981.

6. Haut, R.C. and Crook, R.J.: "Primary Cementing: The Mud Displacement Process," SPE 8253, SPE Annual Technical Conference and Exhibition, Las Vegas, Sept. 23-26, 1979.

7. Clark, C.R. and Carter, L.G. "Mud Displacement with Cement Slurries," SPE 4090, SPE Annual Fall Meeting, San Antonio, Oct. 8-11, 1972.

8. McLean, R.H. et al. "Displacement Mechanics in Primary Cementing," SPE 1488, California Regional SPE Meeting, Santa Barbara, Nov. 17-18, 1966.

9. Tehrani, A. et al. "Laminar Displacement in Annuli: A Combined Experimental and Theoretical Study," SPE 24569, SPE Annual Technical Conference and Exhibition, Washington D.C., Oct. 4-7, 1992.

10. Landau, L.D. and Lifshitz, E.M. "Fluid Mechanics." *Pergamon Press*, London (1959).

11. Cui, H.Q. and Liu X.S. "Research on Helical Flow of Non-Newtonian Fluids in Eccentric Annuli," SPE 29940, International Meeting on Petroleum Engineering, Beijing, Nov. 14-17, 1995

12. Pelipenko, S. and Frigaard, I.A. "Mud Removal and Cement Placement During Primary Cementing of an Oil Well." *Journal of Engineering Mathematics* (Vol. 48, 2004) 1.

13. Escudier, M.P. et al. "Effects of Inner Cylinder Rotation on Laminar Flow of a Newtonian Fluid through an Eccentric Annulus." *International Journal of Heat and Fluid Flow* (Vol. 21, 2000) 92.

14. Escudier, M.P. et al. "Fully Developed Laminar Flow of Purely Viscous non-Newtonian Liquids through Annuli, Including the Effects of Eccentricity and Inner-Cylinder Rotation." *International Journal of Heat and Fluid Flow* (Vol. 23, 2002) 52.

15. Dutra, E.S.S. et al. "Analysis of Interface between Newtonian and Non-Newtonian Fluids Inside Annular Eccentric Tubes," IMECE 59335, ASME Internal Mechanical Engineering Congress, Nov. 13-20, 2004.

16. Li, X. and Novotny R. "Study on Cement Displacement by Lattice-Boltzmann Method," SPE 102979, SPE Annual Technical Conference and Exhibition, San Antonio, Sept. 24-27, 2006.

17. Chin, W.C. "Quantitative Methods in Reservoir Engineering." *Elsevier Science*, Amsterdam (2002).

18. Landrum, W.R. and Turner R.D. "Rotating Liners During Cementing in the Grand Isle and West Delta Area," IADC/SPE 11420, IADC/SPE Drilling Conference, New Orleans, 1983.
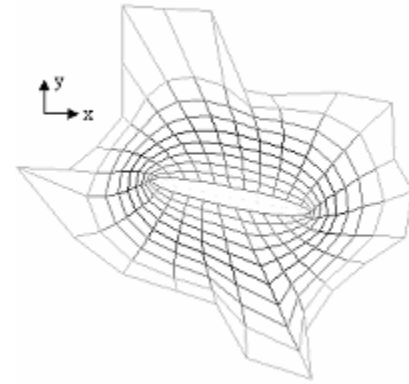
Fig. 1—Example of physical domain in boundary-conforming curvilinear coordinates.
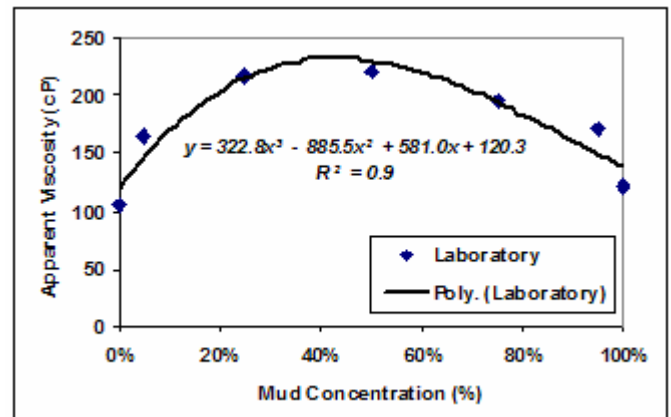

Fig. 2—Example mixing viscosity function where *x* is percent mud in mixture and *y* is apparent viscosity of mixture as determined in the laboratory over a range of fluid combinations.

$$y = 322.8x^3 - 885.5x^2 + 581.0x + 120.3$$
$$R^2 = 0.9$$
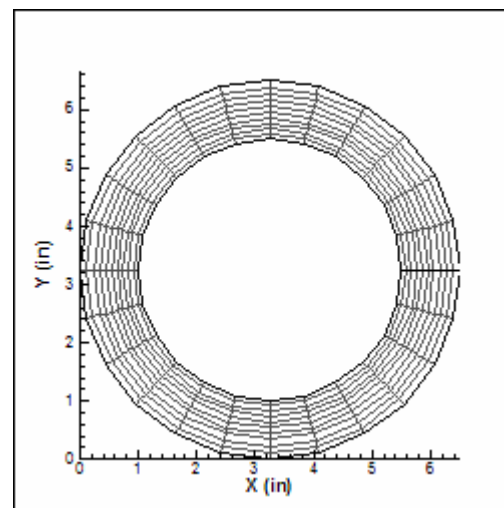
Fig. 3—Baseline 2-D radii grid.
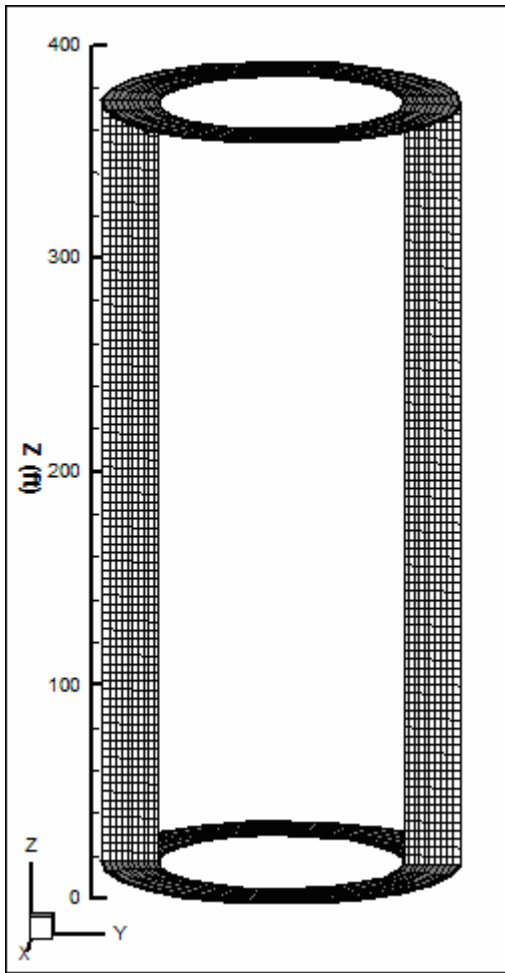
Fig. 4—Baseline 3-D wellbore grid.
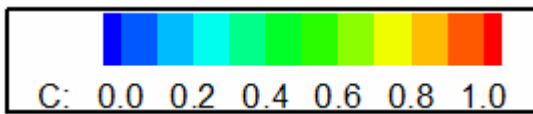
Fig. 5—Mixture legend where *C* represents the displacing fluid concentration.
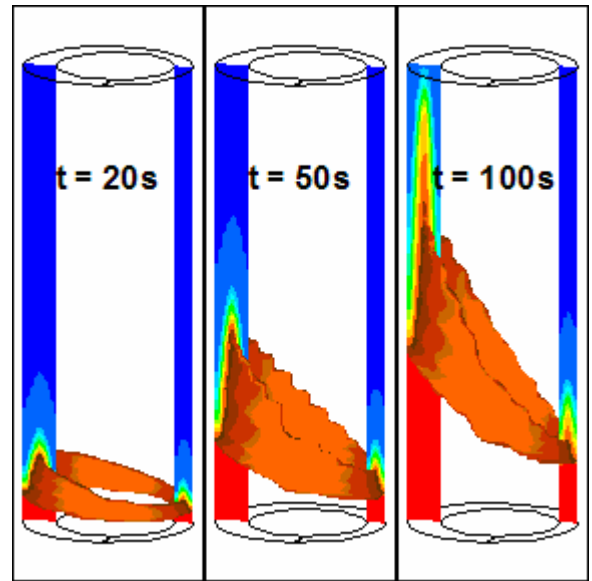
Fig. 6—Concentration profile for 70% casing standoff.
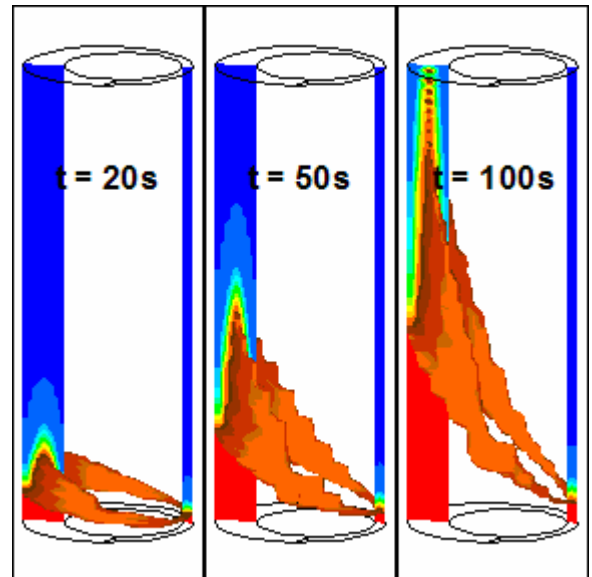
Fig. 7—Concentration profile for 40% casing standoff.
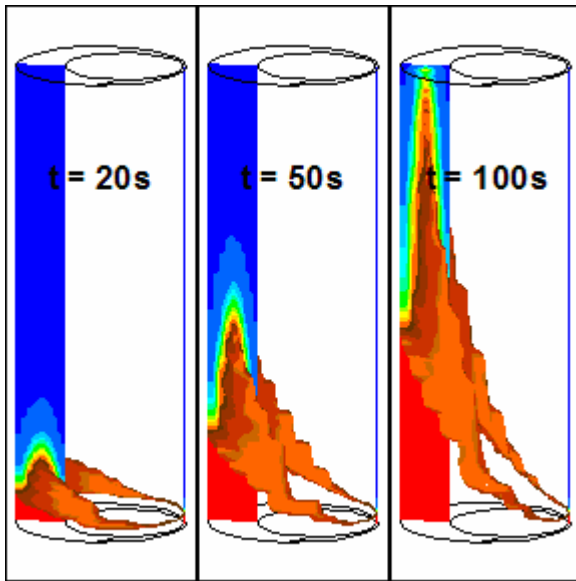
**Fig. 8—Concentration profile for 10% casing standoff.**
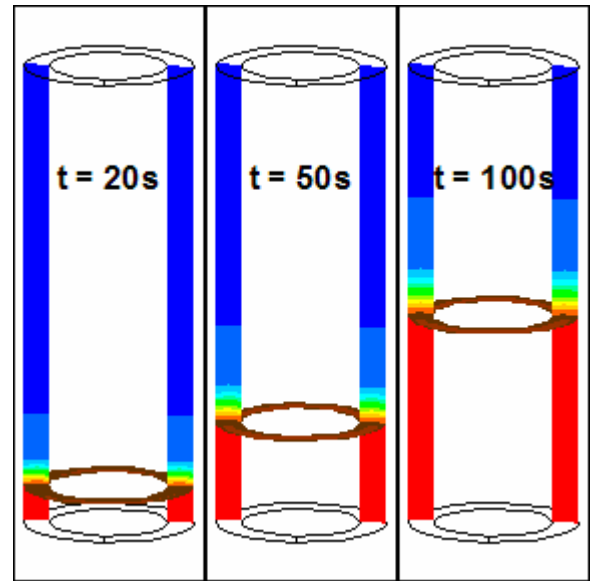
Fig. 10—Concentration profile for D = 3x10^{-2} in.^{2}/sec.
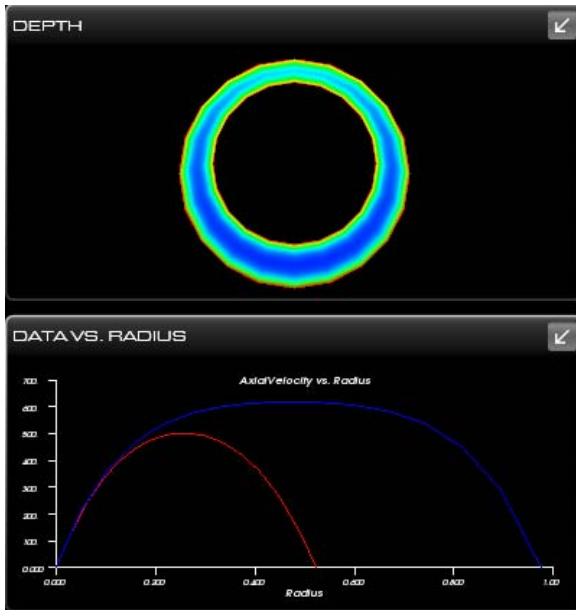
Fig. 9—Velocity profile variances in an eccentric annulus.
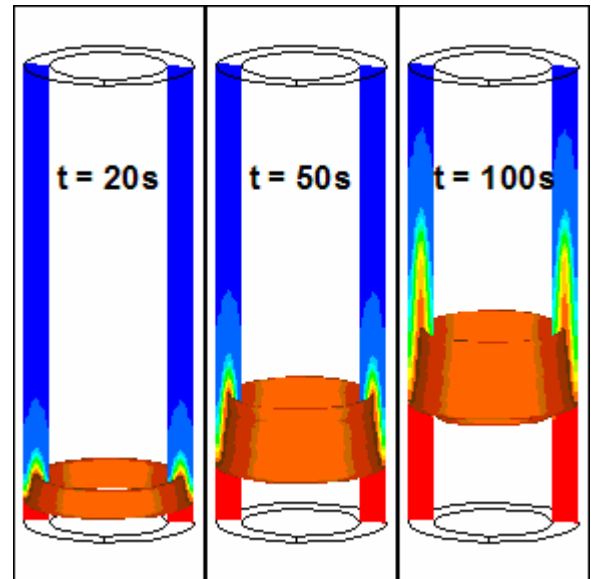

Fig. 11—Concentration profile for D = 3x10^{-4} in.^{2}/sec.
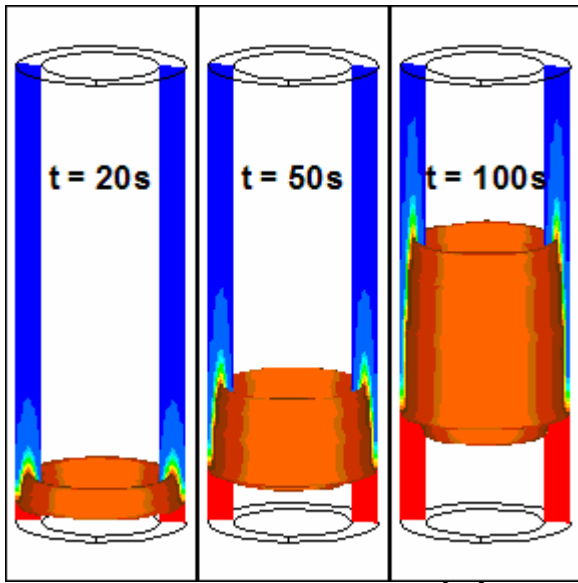
**Fig. 12—Concentration profile for D = 3x10⁻⁶ in.²/sec.**
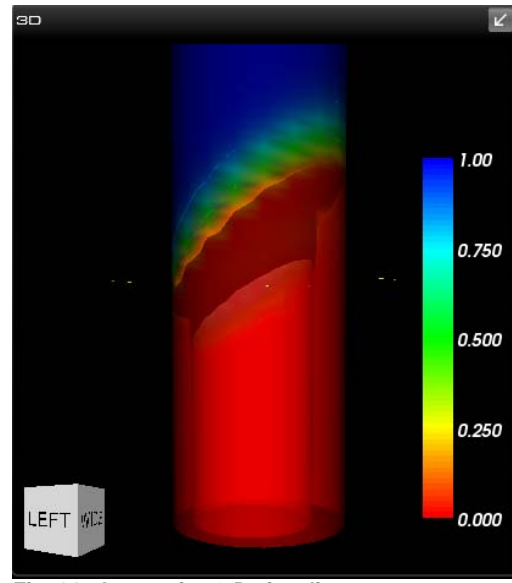
Fig. 14—Interactive 3-D visualizer.
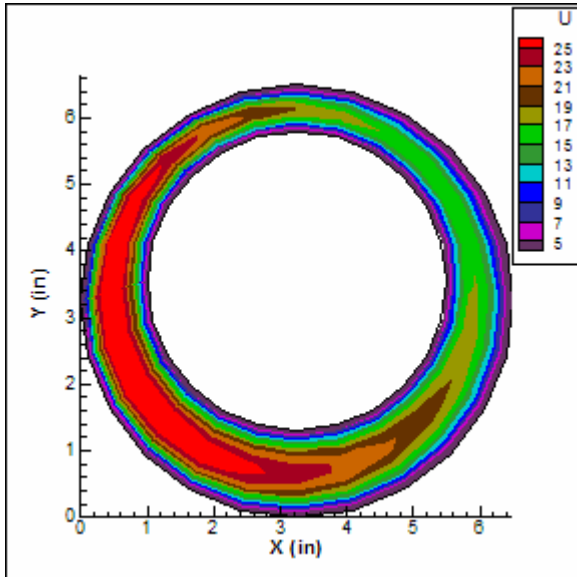
Fig. 13—2-D steady-state velocity profile with inner-casing rotation of 20 RPM in a 70% standoff scenario.